Wind and Structures, *Vol. 17, No. 3(2013) 245-262*
DOI:http://dx.doi.org/10.12989/was.2013.17.3.245

The acrosswind response of the downwind prism in a twin-prism system with a staggered arrangement

Fuh-Min Fang[1], Cheng-Yang Chung[1], Yi-Chao Li[2], Wen-Chin Liu[2] and Perng-Kwei Lei[*3]

[1]*Department of Civil Engineering, National Chung Hsing University, Taichung, Taiwan 40227*
[2]*Architecture and Building Research Institute, Tainan, Taiwan 71150*
[3]*Department of Bio-Industrial Mechatronics Engineering, National Chung Hsing University, Taichung, Taiwan 40227*

(Received December 11, 2011, Revised August 16, 2012, Accepted December 1, 2012)

Abstract. The flow interaction between two identical neighboring twin square prisms in a staggered arrangement in an open terrain was investigated experimentally. The downwind prism was mounted on a rigid-aeroelastic setup in an open-terrain boundary layer flow to measure its acrosswind root-mean-square responses and aerodynamic damping ratios. By varying the relative location of the upwind prism and the Scruton number associated with the downwind prism, the acrosswind aeroelastic behavior of the downwind prism was analyzed and compared to that of an isolated one. Results showed that the acrosswind root-mean-square response of the downwind prism could be either suppressed or enhanced by the wake flow produced by the neighboring upwind prism. Besides the assessment of the wake effect of the downwind prism, finally, regressed relationships were presented to describe the variation of the aerodynamic damping ratio so as to predict its acrosswind fluctuating response numerically.

Keywords: high-rise building; aerodynamic damping; wind tunnel tests

1. Introduction

The acrosswind vibration of a high-rise building is mainly caused by the separation and vortex shedding processes of the wake flow. As the structural response is significant, it can produce a noticeable secondary effect and leads to a change of the wind load and the response. The resulting aeroelastic behavior, caused by the interaction between the motion of wind and the structure, can significantly promote the extent of the structural response under certain critical conditions. Therefore, its analysis becomes important in the consideration of building serviceability or even structural safety for high-rise building designs.

There have been a number of studies regarding the acrosswind aeroelastic phenomena of a single high-rise building. Typically, Matsumoto (1986) used the data from aerodynamic and aeroelastic tests to show that, for a rectangular cylinder with an aspect ratio of 4 and a cross-sectional depth-to-width ratio of 0.6 and 1.0, the acrosswind vibration exhibited instability in

*Corresponding author, Professor, E-mail: g9462209@mail.nchu.edu.tw

http://www.techno-press.org/?journal=was&subpage=8 ISSN: 1226-6116 (Print), 1598-6225 (Online)

an α=0.2 boundary-layer flow. Watanabe *et al*. (1997) proposed empirical aerodynamic damping impedance functions to simulate aerodynamic damping of tall buildings. Based on the measurement results from a pressure model with a square cross-section, Cheng *et al*. (2002) performed aeroelastic model tests to study the acrosswind response and aerodynamic damping of isolated square-shaped high-rise buildings. It was found that in open terrains the acrosswind response could be categorized into three regions based on the building's mass-damping coefficient. Based on the measurement results of windward and leeward surfaces of a rectangular building model, Gabbai and Simu (2010) proposed a method to estimate the aerodynamic damping and building response in the along-wind direction.

Several other experimental studies were conducted in cases of non-isolated buildings. Bailey (1985) investigated the along-wind and acrosswind responses of a tall square model building under interference excitation and proximity effects of two neighboring buildings and found that both the upstream and downstream buildings were affected and critical relative building locations were identified. Sakamoto and Haniu (1988) measured the winds loads of two identical square prisms in a turbulent boundary layer. The resulting mean and fluctuating forces on the prisms revealed that the phase shift between the fluctuating lifts acting on the twin prisms in a tandem arrangement was proportional to the gap distance. In addition, the distributions of the fluid forces and the corresponding Strouhal number are presented and classified into several regions. Taniike and Inaoka (1988) examined the mutual interference between two rectangular buildings with different sizes. It was found that with a small gap distance the acrosswind response of the downstream building could increase significantly due to switching excitation produced by the interference effect. The result of the extended study by Taniike (1992) indicated that the fluctuating forces on the downstream building generally increased by the presence of the upstream building.

Furthermore, Khanduri *et al*. (1998) reviewed the work pertaining to the interference effect among neighboring structures and proposed certain general guidelines in help with practical design and planning. More recently, Huang and Gu (2005) measured the wind loads and dynamic responses of two identical building models with square cross-sections and proposed along-wind and acrosswind dynamic interference factor contours to be used for wind load codes of buildings.

Blazik-Borowa (2006) proposed a quasi-steady model of vibrations of two cylinders in a side-by-side arrangement. Kumar and Gowda (2006) investigated the interference effect between two neighboring twin square cylinders in a uniform flow and indicated that there was a critical combination of the gap distances that lead to maximum vibration amplitude of the upstream cylinder. Lim and Bienkiewicz (2007) studied the effect of structural coupling on the wind-induced response of twin tall building connected by a skybridge. Zhang and Gu (2008) examined the pressure distributions on two adjacent buildings in a staggered arrangement and presented a numerical method for the pressure predictions with a SIMPLEC-type algorithm.

The present study concentrates on experimental investigations of the aeroelastic behavior of a high-rise building affected by the wake flow of neighboring structures. In particular, the analysis involves a pair of identical square prisms with a staggered arrangement in a boundary-layer flow in open terrains. By varying the relative location of the upwind prism, a rigid aeroelastic building model was set at the downwind prism to measure its tip deflections at various approaching wind speeds. Besides the examination of the aeroelastic behavior of the downwind prism, including the tip root-mean-square responses and the corresponding aerodynamic damping ratios, due to different conditions of wake effects, three types of dynamic characteristics associated with the elastic model in terms of Scruton numbers were employed to analyze the results of the acrosswind model responses.

2. Description of experiments

The aeroelastic tests were performed in the test section (4 m×2.6 m×35 m) of the boundary layer wind tunnel at Architecture and Building Research Institute (ABRI). Four spires (bottom width=0.3 m; height=1.6 m) were installed at the upstream and followed by a number of roughness blocks (0.14 m×0.07 m×0.0 5m) spaced evenly (center-to-center distance=0.8 m) at the tunnel floor area with a longitudinal length of 16.4 m. The atmospheric boundary layer flow was generated to represent the condition of an open terrain. The mean and fluctuating velocity profiles of the approaching flow are depicted in Fig. 1. For the mean profile, the corresponding power-law α value is 0.14 and the boundary layer thickness (δ) is about 150 cm.

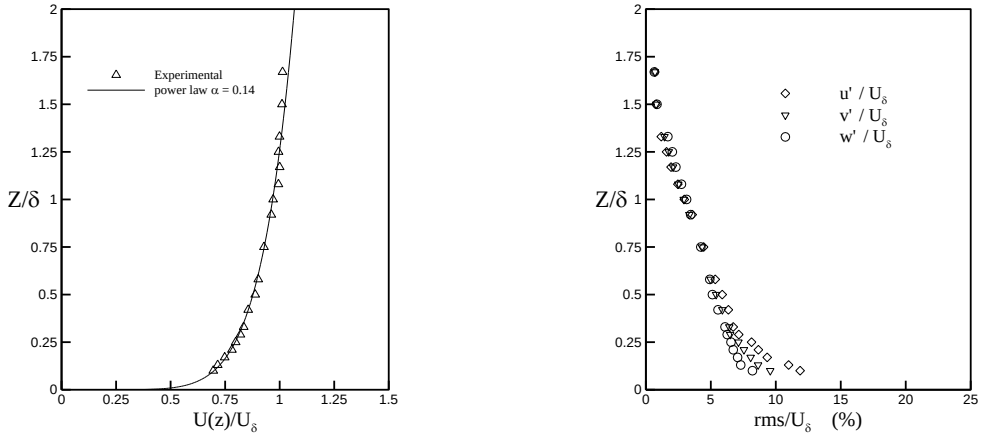

Fig. 1 Velocity profiles of the approaching flow

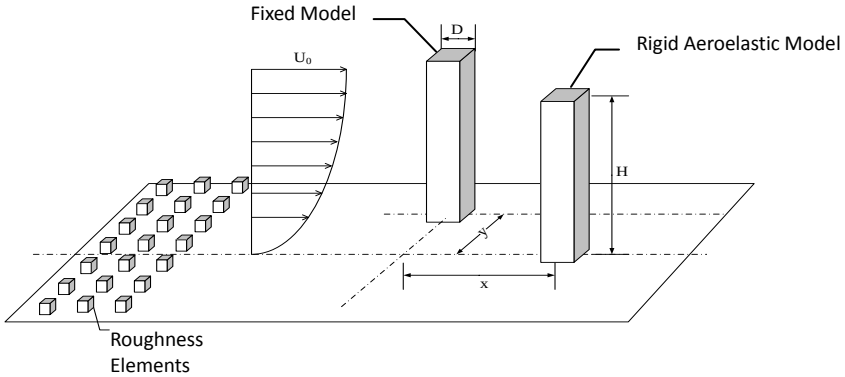

Fig. 2 Schematic of the experimental program

2.1. Model arrangements

Two identical square prisms with an aspect ratio (H/D) of 7 were set in a staggered arrangement

(see Fig. 2). The upwind prism was fixed on the tunnel floor and the downwind prism was mounted on an elastic model setup. The models were rigid with a width (D) and height (H) respectively of 13 cm and 91 cm. The blockage ratio of the model experiments was less than 5%.

The gap distances between the centers of the prisms (x and y) varied from 2D to 5D and 0 to 2D, respectively. During the tests, the approaching-flow velocity at a height of H, denoted by U_o, varied from about 3 m/s to 24 m/s.

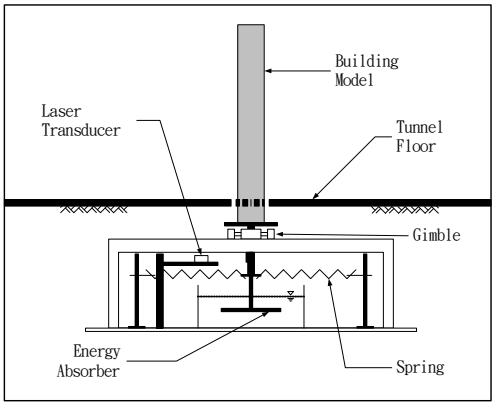

Fig. 3 Setup of rigid-aeroelastic-model

2.2. Rigid-aeroelastic-model setup

At the bottom of the downwind prism, a dual axes mechanism, allowing for two sway modes of vibration, was employed (see Fig. 3). Two sets of springs were connected with an extension rod to simulate the structural stiffness in the along-wind and acrosswind directions. At the end of the rod, a disk was immersed in a container filled with viscous oil to reflect the structural damping of the prism. In the model tests, the stiffness and structural damping were the same in both the along-wind and acrosswind directions. Laser transducers were installed to monitor the deflection history of the extension rod of the downwind prism and the model tip response was further obtained by geometry. The fundamental frequencies of the elastic model (f_m) in both the directions were 3.75 Hz.

In the experiments, the Scruton number was determined as

$$Scr = \frac{m^*}{\int_0^H \varphi^2(y)dy} \frac{\xi_m}{\rho D^2} \tag{1}$$

where m* and φ denote respectively the generalized mass and modal shape; ρ is air density (1.20 kg/m^3) and ξ_m is the structural damping ratio. By assuming that the building model is uniform, Eq. (1) becomes

$$Scr = \frac{m_m}{\rho D^2} \xi_m \tag{2}$$

where m_m denotes the mass of model per unit height. With an averaged mass density of model (141.3 kg/m^3), m_s then equals to 2.388 kg/m. Table 1 illustrates the related properties of the aero-elastic model tests. According to the previous results for an isolated prism by Cheng *et al*. (2002), the three selected Scruton numbers (6.74, 3.15 and 1.18) are respectively in the aerodynamically stable, aerodynamically unstable and aerodynamic divergence regions.

2.3. Determination of the aerodynamic damping ratio

In the aeroelastic experiments, the net damping ratio (ξ_{net}) was determined by the logarithmic decrement method. At each experiment, an initial across-wind deflection (about 0.2D at the top of the prism) was prescribed at the beginning. By examining the transverse deflection history of the prism after it was released, the decay rate (δ) was evaluated as the logarithmic value of the ratio of two successive peak deflections and the corresponding net damping ratio was found according to Eq. (2) as

$$\delta = \frac{2\pi \xi_{net}}{\sqrt{1-\xi_{net}^2}} \tag{3}$$

The aerodynamic damping ratio (ξ_a) was then obtained as the result of the net damping ratio (ξ_{net}) subtracted by the structural damping ratio (ξ_m).

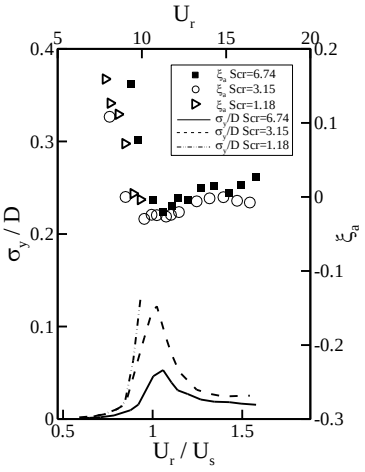

Fig. 4 Acrosswind response and aerodynamic damping of an isolated prism

3. Results

3.1. Acrosswind response and aerodynamic damping ratio of an isolated prism

For comparison purposes, aeroelastic experiments of an isolated prism were performed at the beginning. Fig. 4 shows the acrosswind root-mean-square tip responses of the single prism (σ_y) at

various wind speeds in the cases of the three selected Scruton numbers. In addition, the corresponding variations of aerodynamic damping ratio (ξ_a) are also presented. In the figure, the approaching wind speed, at a height of H, is normalized in two ways. One is in a form of a reduced velocity ($U_r=U_o/f_mD$, where f_m is the model frequency) and the other is in terms of U_r/U_s ($=f_s/f_m$), where $U_s=U_o/f_sD$ and f_s is the shedding frequency.

In all the three Scruton number cases, the general tendency of the experimental results indicates that the aerodynamic damping ratio decreases sharply as U_r increases at low wind speeds. When U_r reaches about 10.5, the aerodynamic damping ratio becomes a minimum. As the wind speed increases further, ξ_a increases mildly at the two larger Scruton numbers (6.74 and 3.15). On the other hand, the acrosswind root-mean-square tip response (σ_y) increases with an increase of the wind speed. At the two larger Scruton numbers, peak responses are detected when minimum values of ξ_a occur (U_r=10.5) due to the effect of resonance. As U_r exceeds the lock-in range, σ_y then decreases with an increase of the wind speed. Particularly in the case Scr=1.18, σ_y becomes substantially large near the resonance speed compared to the other two cases. The measurement fails to obtain the data of σ_y and ξ_a at high wind speeds due to the limitation of the measurement devices.

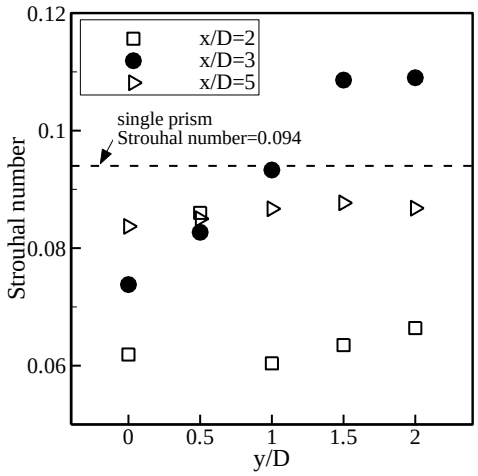

Fig. 5 Strouhal numbers of the downwind cylinder for twin prisms

3.2. Strouhal number of downwind prism in the twin-prism system

Aerodynamic model tests were also conducted by using a six-beam force balance to measure the wind loads of the downwind prism in the twin-prism system. Fig. 5 depicts the variations of the resulting Strouhal number ($St = f_mD/U_o$) in various spatial arrangements of the twin prisms. As the normalized longitudinal gap distance (x/D) is equal to 2 and 5, the variations of St appear mild. Compared to the single fixed prism result (0.094), the Strouhal numbers are relatively smaller (about 0.064 and 0.085). On the other hand, when x/D=3, St generally increases as the normalized traverse gap distance (y/D) increases.

It is noted that the experimental result from Kumar and Gowda (2006) of a uniform flow past a

two-dimensional square cylinder indicated that the Strouhal number was 0.13. In contrast, the resulting Strouhal number in the present study of a surface-mounted square prism with a finite height (H=7D) is relatively smaller (0.094). The difference should be attributed to the outcome of three-dimensional flow effects.

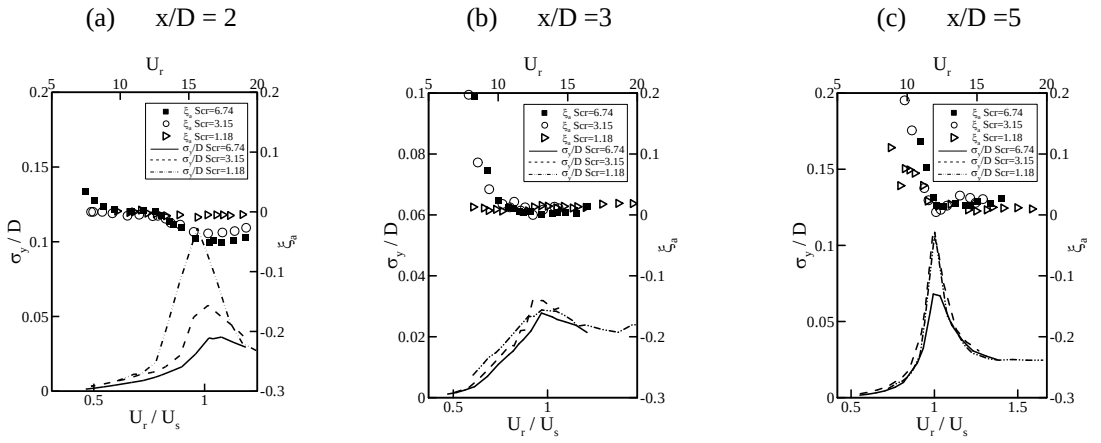

Fig. 6 Variations of RMS tip response and aerodynamic damping ratio (y/D=0)

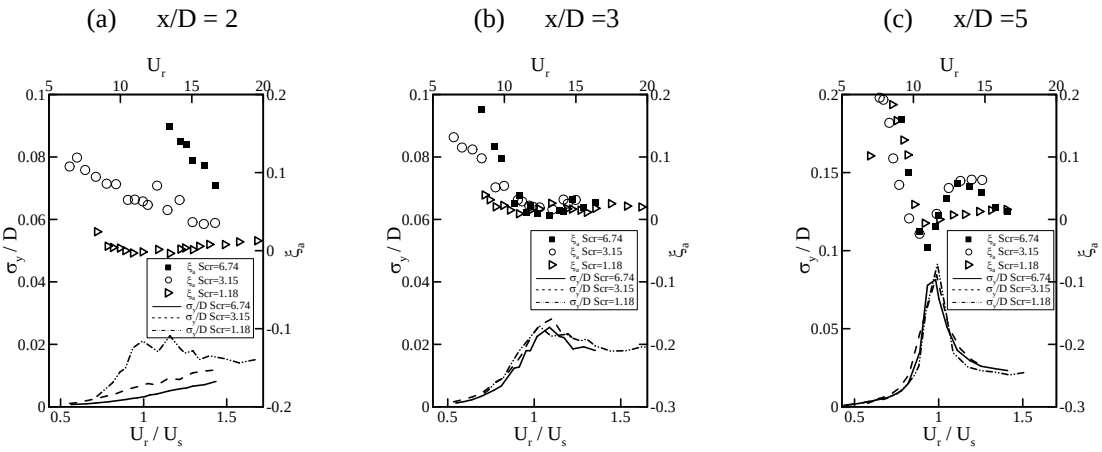

Fig. 7 Variations of RMS tip response and aerodynamic damping ratio (y/D=0.5)

3.3. Acrosswind response of downwind prism in twin-prism system

Figs. 6 to 10 show the measurement results of the downwind prism in the twin-prism system. In the cases that the normalized longitudinal distance (x/D) equals 2, peak root-mean-square tip

deflections are detected at the resonance speed (U_s) in a tandem arrangement (y/D=0; Fig. 6(a)) at all the three Scruton numbers. Generally, the one with a smaller Scr value leads to a greater tip response. The tendency of the response variations appears similar to that of the single prism (Fig. 4). However, the magnitudes of the root-mean-square deflections appear smaller due to the wake effects produced by the upwind prism. Moreover, in contrast to the single-prism case, the response does not diverge as *Scr*=1.18. As the normalized traverse distance (y/D) extends to 0.5, the acrosswind root-mean-square deflections are significantly reduced (Fig. 7(a)). Although the root-mean-square response is the largest as Scr=1.18, the significance of the peak becomes weak. Also, at the other two Scruton numbers (6.74 and 3.15), no peaks occur within the test range.

Furthermore, as y/D exceeds 1, σ_y diverges at large wind speeds in all the three Scr cases (Figs. 8(a) to 10(a)).

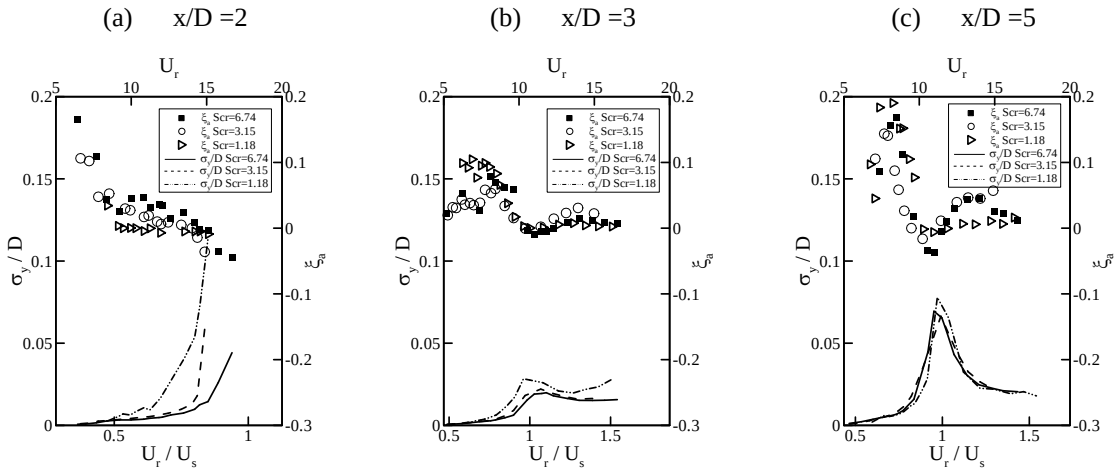

Fig. 8 Variations of RMS tip response and aerodynamic damping ratio (y/D=1)

When x/D=3, a tendency of reduction in terms of σ_y is detected again as y/D is less than or equal to 1 (Figs. 6(b) to 8(b)) and the corresponding root-mean-square responses appear insensitive to the change of Scr. However, as y/D is greater than 1.5, σ_y diverges again at all the three Scruton numbers (Figs. 9(b) and 10(b)).

In the cases x/D=5, the upstream wake effect becomes relatively weaker and the resulting acrosswind tip response appear to regain its significance. Peak values are detected at the resonance wind speed and σ_y does not diverge within the test ranges in all the cases. Except in the tandem case (y/D=0) that a smaller response is obtained as *Scr*=6.74 than those of the other two Scr cases (Fig. 6(c)), the change of Scr value does not appear to significantly affect the variations of σ_y .

Based on the magnitudes of the root-mean-square deflections, the results can be generally classified into stable and diverged regions in terms of σ_y in relation to the spatial gap distances between the twin prisms (see Table 2). That is, the resulting acrosswind root-mean-square responses of the downwind prism are finite at the resonance wind speed as the spatial distances fall in the stable region. Otherwise, the responses diverge within the test wind speed range in all the

three cases of Scruton numbers.

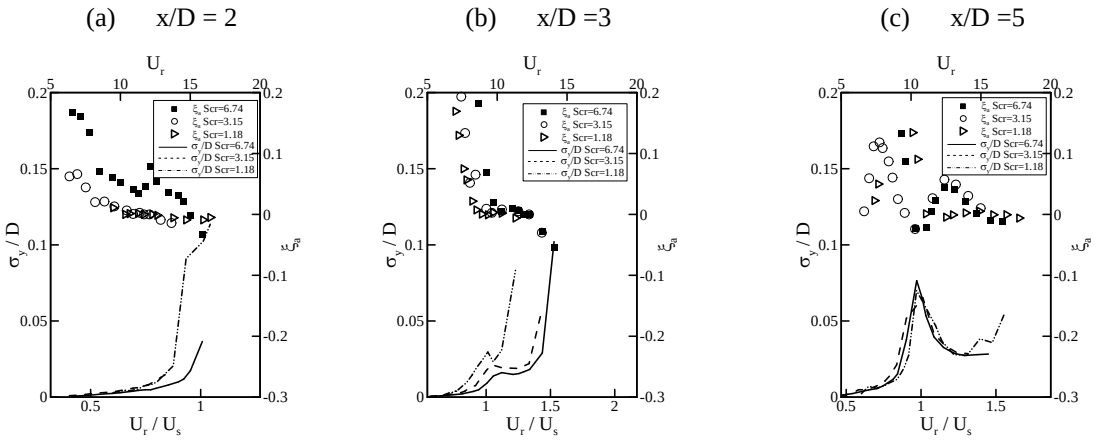

Fig. 9 Variations of RMS tip response and aerodynamic damping ratio (y/D=1.5)

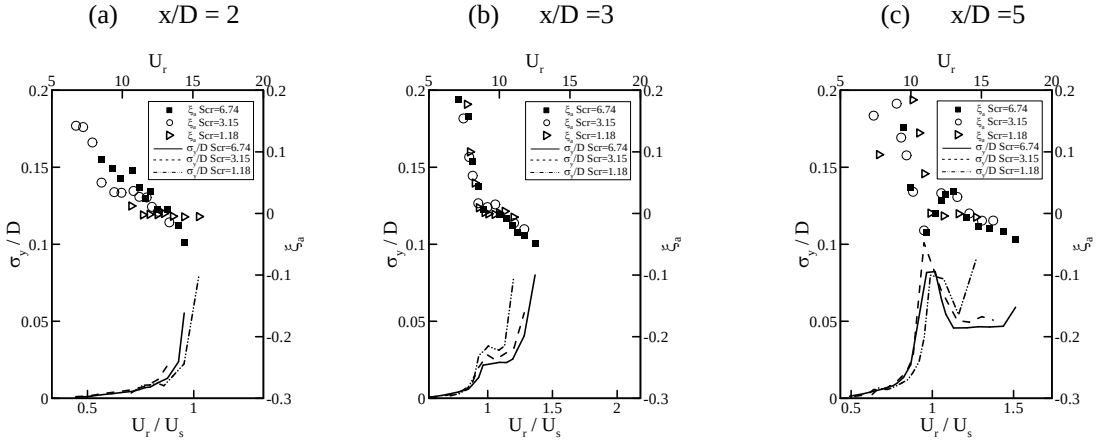

Fig. 10 Variations of RMS tip response and aerodynamic damping ratio (y/D=2)

Table 1 Properties of the aero-elastic test models

Scruton number	Model density ρ_m (kg/m^3)	Structural frequency f_m (Hz)	Damping ratio ξ_m (%)
6.74	141.3	3.75	5.72
3.15	141.3	3.75	2.68
1.18	141.3	3.75	1.00

Table 2 Patterns of resulting root-mean-square acrosswind tip responses

y/D x/D	0	0.5	1	1.5	2
2	Stable	Stable	Diverged	Diverged	Diverged
3	Stable	Stable	Stable	Diverged	Diverged
5	Stable	Stable	Stable	Stable	Stable

4. Prediction of the acrosswind response of the downwind prism

Due to the complexity of the wake flow produced by the upstream prism, it leads to different acrosswind response patterns of the downstream prism (Fig. 6 to Fig. 10). It is therefore interesting to develop a useful way to evaluate the acrosswind response of the downwind prism. Accordingly, a step-by-step integration method was adopted to predict the acrosswind root-mean-square tip response of the downwind prism.

The concept of the prediction method follows that was brought up by Cheng *et al*. (2002). As the part of the interactive wind force is moved to the left-hand-side of the dynamic incremental-equilibrium equation, it becomes

$$\ddot{\theta}+2\,\xi_{net}\,\omega\dot{\theta}+\omega^2\theta=\frac{M}{I_{O-O}} \tag{3}$$

where θ, $\dot{\theta}$ and $\ddot{\theta}$ denote respectively the acrosswind angular deflection, speed and acceleration. ω is the angular frequency of the downwind prism. I_{O-O} is the moment of inertia at the base; M is the base moment, which can be obtained from the aerodynamic test results. On the other hand, the net damping ratio (ξ_{net}) is the sum of the structural and aerodynamic damping ratios (ξ_m and ξ_a). Since the aerodynamic damping ratio varies with different approaching wind speeds as well as the relative location of the upwind prism, it is then necessary to search for a convenient expression of the variation of the aerodynamic damping ratio.

In the prediction, the calculation was set at an initial time and the instantaneous vibrating speed and deflection were used as the initial condition. By using the base moment results from the force-balance measurements with corresponding net damping ratio, the changes within a calculation period were computed to further update the vibrating speed and deflection at the next time step. On the other hand, the variations of the aerodynamic damping ratio were obtained by regression based on the measurement results (Figs. 6 to 10). Accordingly, iterations were performed to predict the histories of the acrosswind tip responses of the downwind prism at all wind speeds within the range of interest.

4.1. Prediction of downwind prism response in the diverged regions

Based on the experimental results in the cases with diverged responses (see Table 2), Fig. 11 shows the variations of the aerodynamic damping ratio (ξ_a) with respect to the reduced velocity. For better predictions, it is found that the regressions have to be performed in two groups in terms of the Scruton numbers and the regression relationships are

$$\xi_a = -0.1\,U_r + 1.05 \quad (U_r < 10.5) \qquad \text{for } Scr = 1.18$$
$$-0.0012\,U_r + 0.0126 \quad (U_r \geq 10.5) \tag{4}$$

$$\xi_a = -0.1\,U_r + 1.05 \quad (U_r < 10.5) \qquad \text{for } Scr = 3.15 \text{ and } 6.74$$
$$-0.017\,U_r + 0.1785 \quad (U_r \geq 10.5) \tag{5}$$

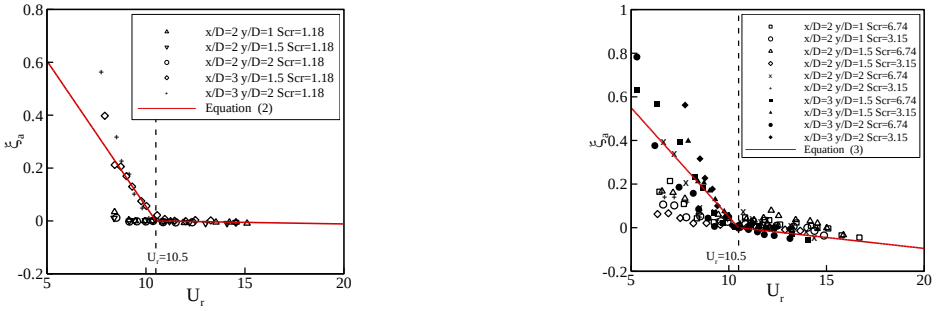

(a) Scr = 1.18 (b) Scr = 3.15 and 6.74

Fig. 11 Variations of aerodynamic damping ratio and the regressions in diverged regions

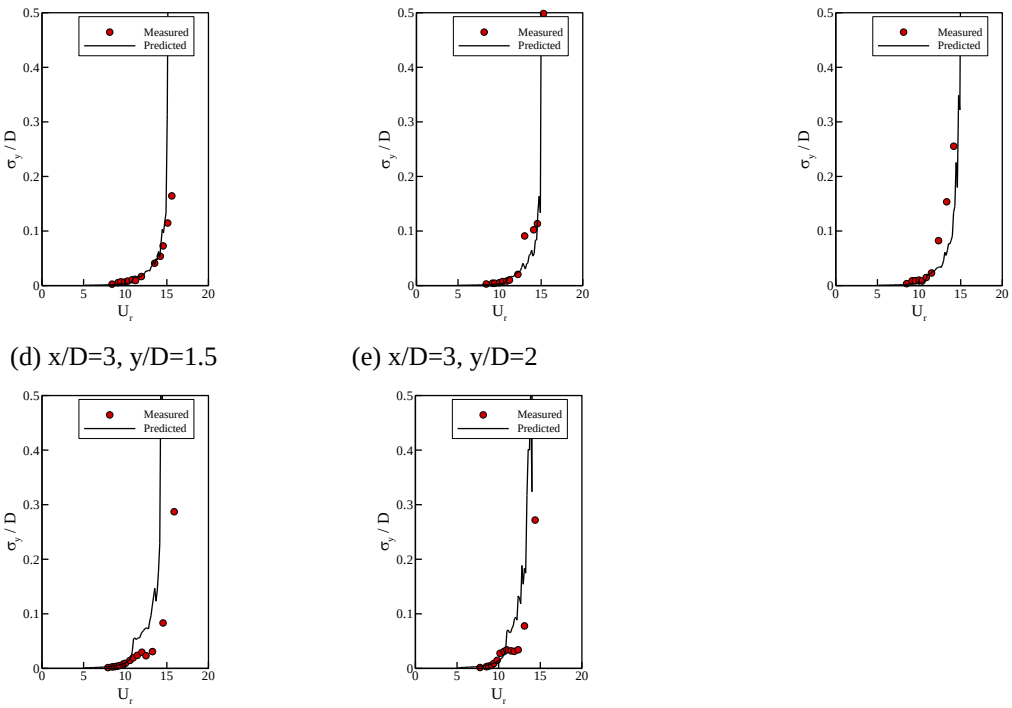

Fig. 12 Comparison of acrosswind RMS responses in diverged regions (Scr=1.18)

Figs. 12 to 14 illustrate the comparisons of the experimental and the predicted variations of the acrosswind root-mean-square tip responses of the downwind prism at the three Scruton numbers. The comparisons show that that the predictions are in reasonable agreement with the measurement results.

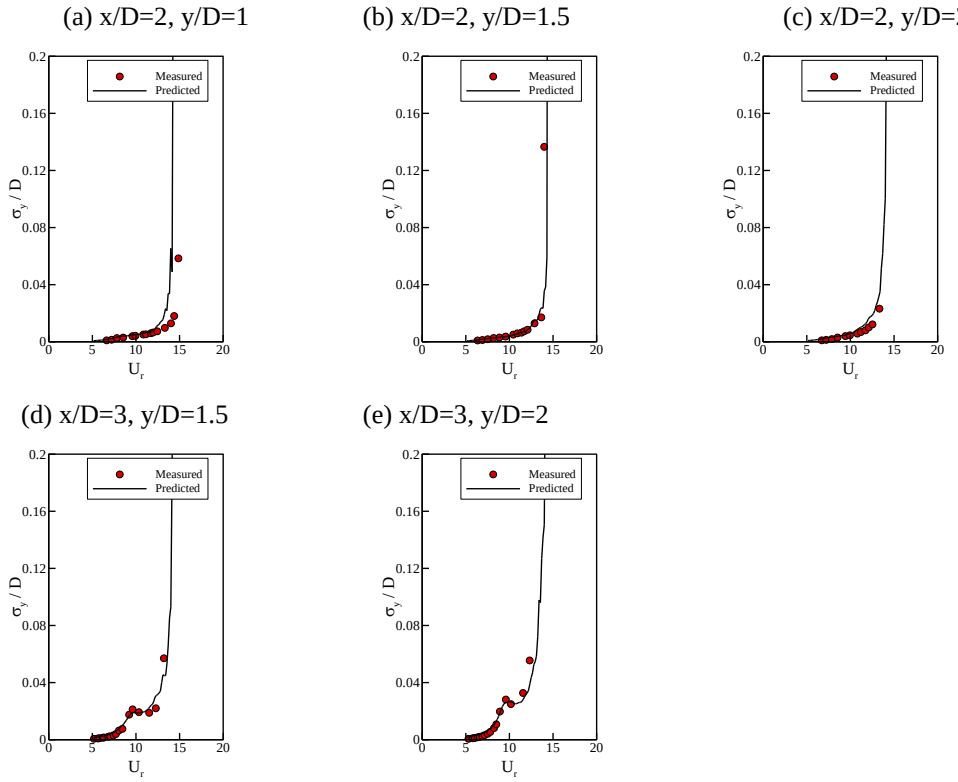

Fig. 13 Comparison of acrosswind RMS responses in diverged regions (Scr=3.15)

4.2. Prediction of downwind prism response in the stable regions

In the cases without diverged responses, experimental results show that at all the three Scruton numbers the variations of the normalized aerodynamic damping ratio (ξ_a/ξ_s, where ξ_s is the aerodynamic damping ratio at the resonance stage) generally follows a similar tendency if it is plotted against U_r-U_s (Fig. 15). Accordingly, the corresponding regression relationship is obtained as

$$\xi_a = 0.05 \times \xi_s \left[(U_r - U_s)^2 - 0.7 \right] \tag{6}$$

Figs. 16 to 18 show the comparisons of the experimental and the predicted results at the three Scruton numbers. The predictions are considered fairly well.

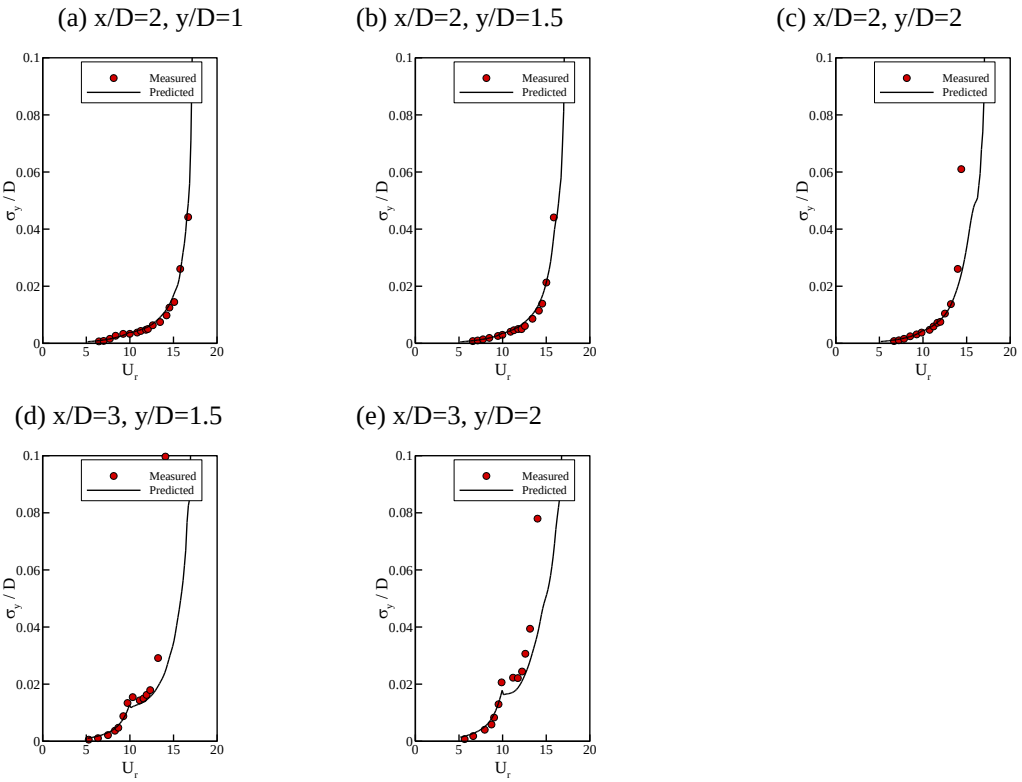

Fig. 14 Comparison of acrosswind RMS responses in diverged regions (Scr=6.74)

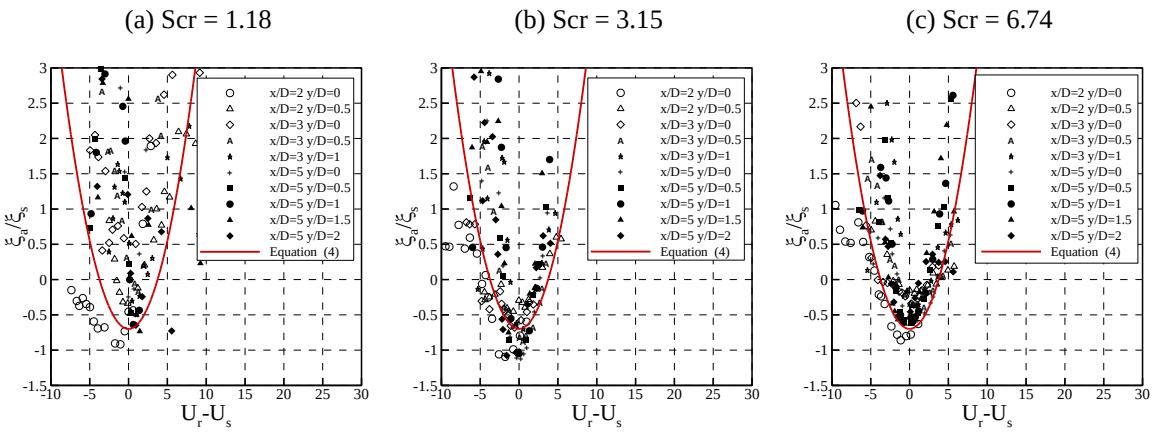

Fig. 15 Variations of aerodynamic damping ratio and the regressions in stable regions

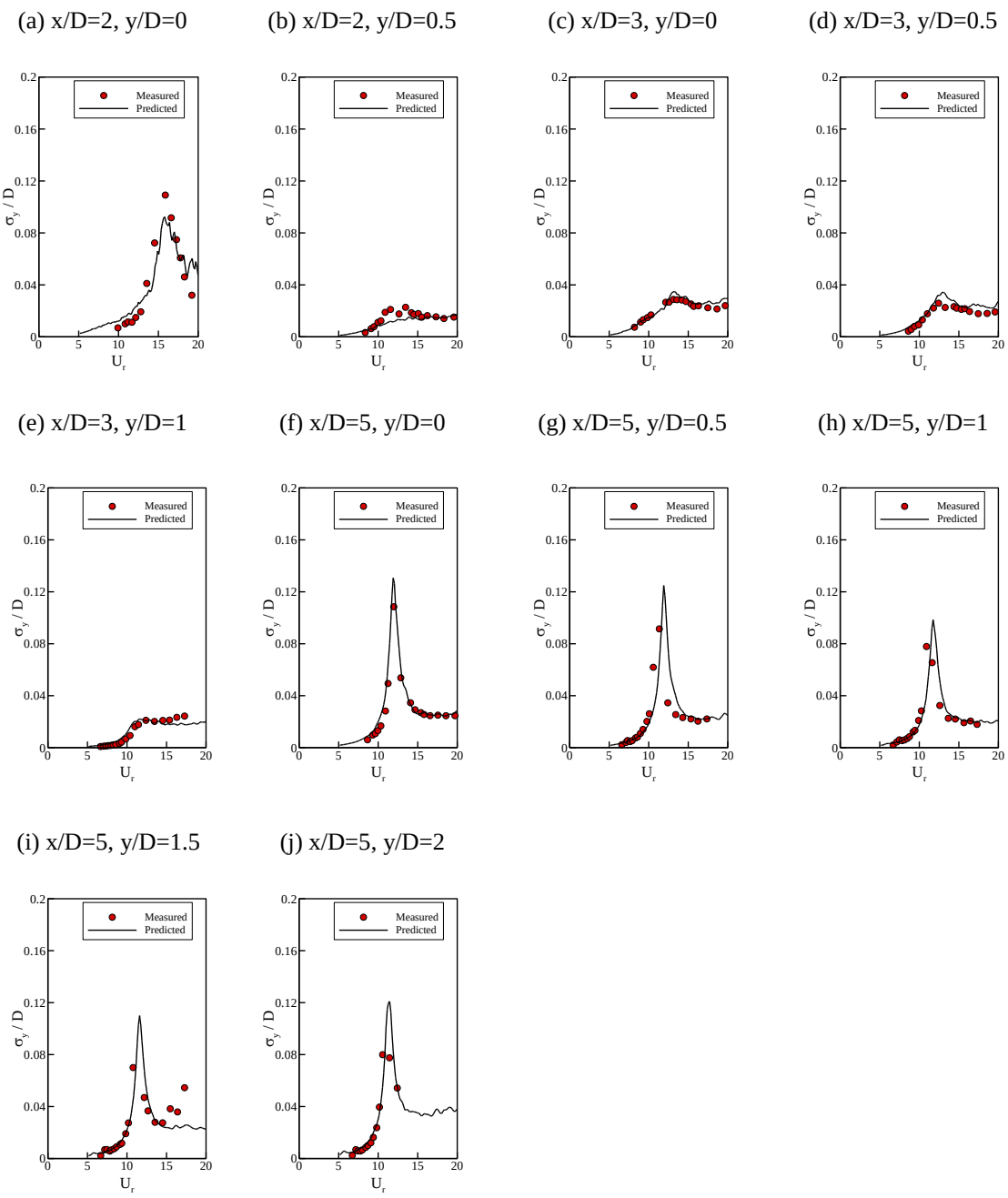

Fig. 16 Comparison of acrosswind RMS responses in stable regions (Scr=1.18)

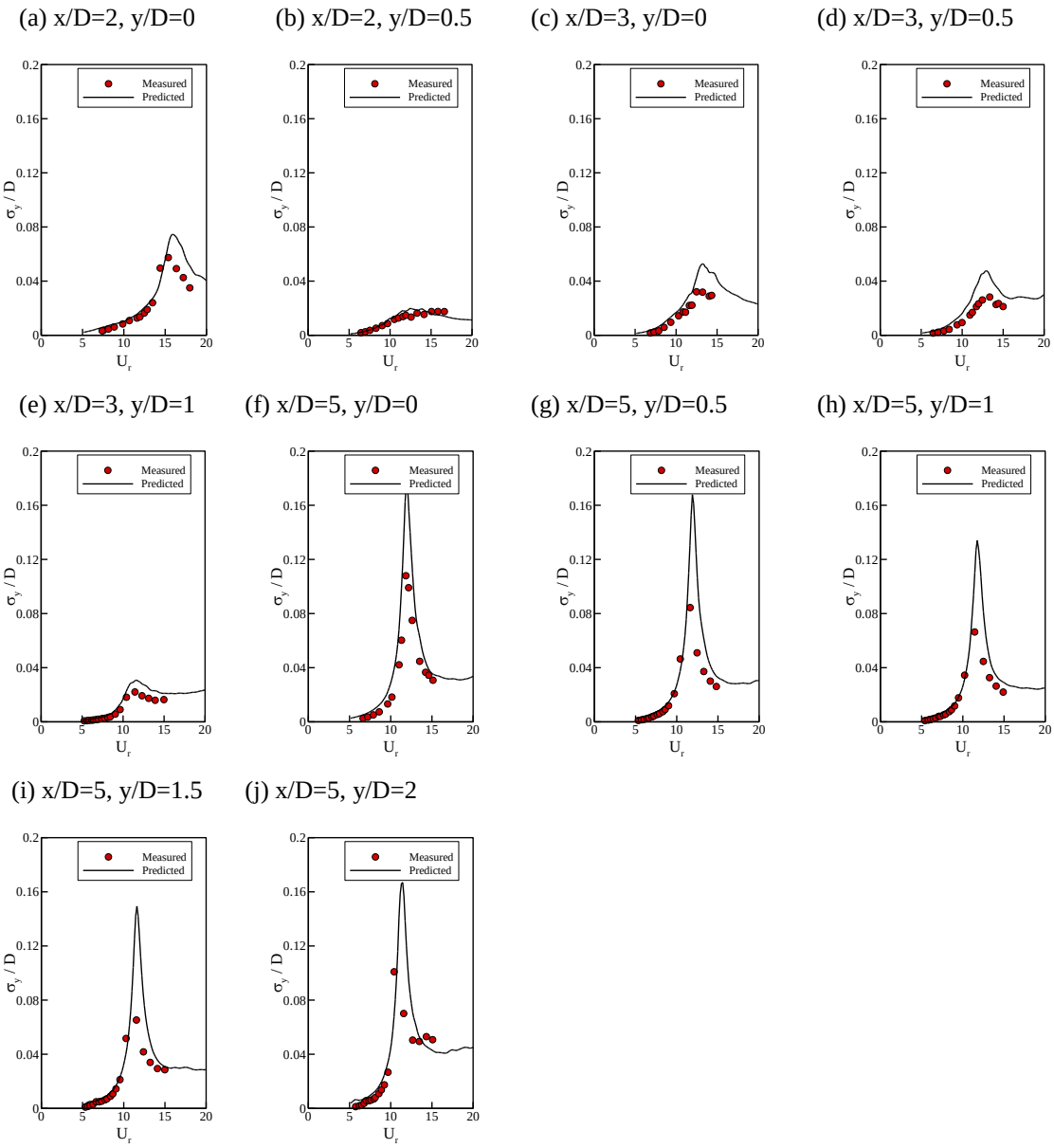

Fig. 17 Comparison of acrosswind RMS responses in stable regions (Scr=3.15)

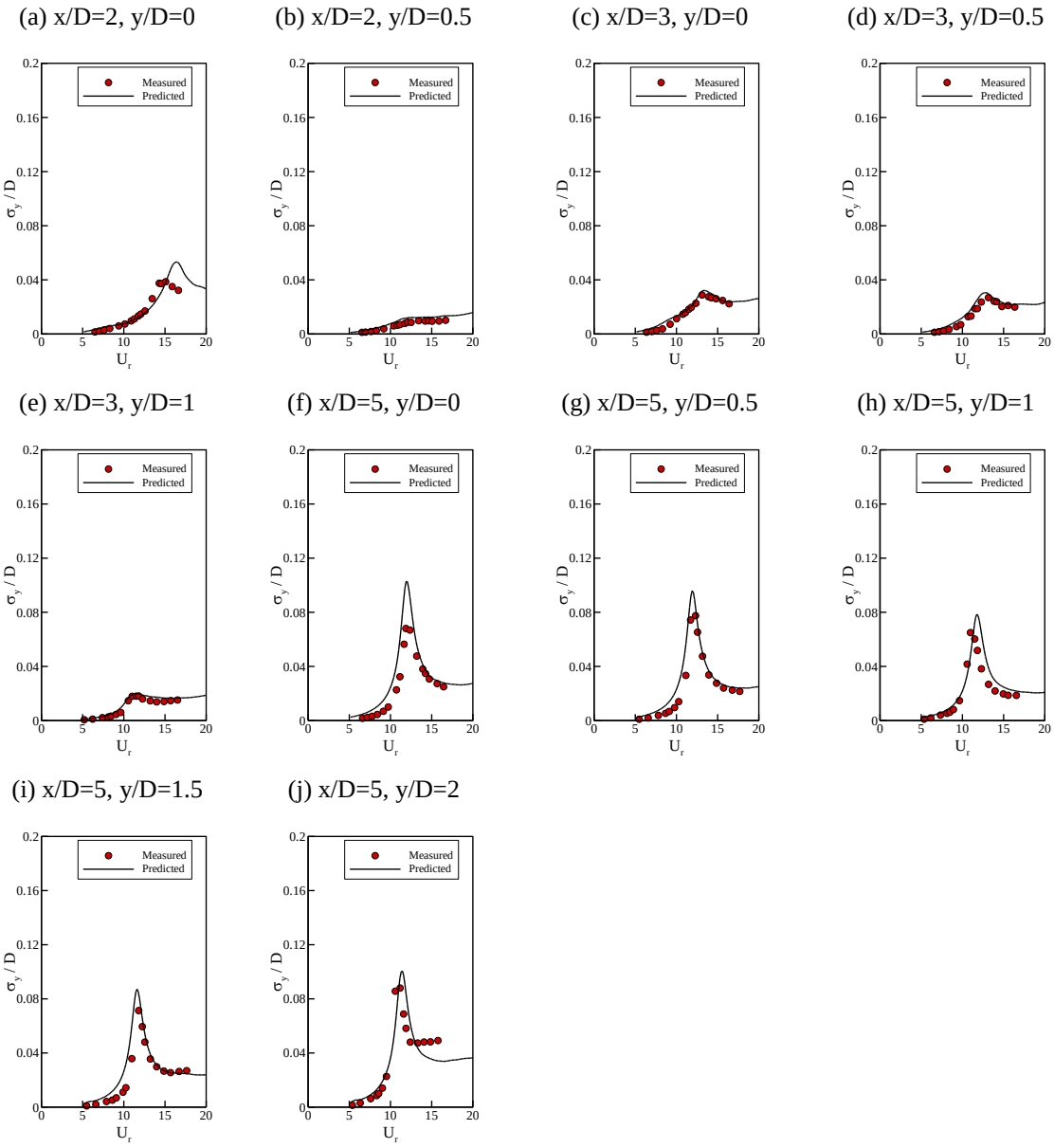

Fig. 18 Comparison of acrosswind RMS responses in stable regions (Scr=6.74)

5. Conclusions

The flow between two identical neighboring twin square prisms in a staggered arrangement is rather complex. As the flow passes the upwind prism, the resulting wake flow produces different types of wind loads and lead to different responses of the downwind prism, depending on the relative spatial locations of the two prisms. Since the structure serviceability is most concerned in the design consideration of building for high-rise buildings, the present study concentrates on the analysis of the building response. Beside the acrosswind structural response patterns of the downwind prism due to the existence of the wind one are examined extensively, the variations of the aerodynamic damping, which describe the feature of the interactive effect of the problem, are assessed. Future studies are suggested to explore the flow physics in more detail. The results would be helpful to explain the experimental results obtained in the study.

Several conclusions are summarized as follows:

(1) With the prescribed approaching boundary-layer flow subject to an open terrain, the acrosswind root-mean-square tip response of an isolated prism diverges as Scr=1.18 within the test ranges. On the other hand, stable results are found at the two larger Scruton numbers (6.74 and 3.15).

(2) In the twin prism system with a staggered arrangement, the acrosswind root-mean-square response of the downwind prism can be affected by the wake flow produced by the neighboring upwind prism. Depending on the gap distances between the twin prisms, the response of the downwind prism can be either suppressed or promoted by the wake effect.

(3) The upwind wake can affect the Strouhal number of the downwind prism. When x/D is equal to 2 or 5, the variation of St is insensitive to the change of y/D. In addition, the corresponding values (about 0.064 and 0.085) are smaller than that of the single-prism result (0.094). When x/D=3, however, St increases as the traverse distance (y/D) increases.

(4) Stable and diverged regions are identified based on the prism gap distances, indicating that the acrosswind root-mean-square tip response of the downwind prism is finite or diverges within the test range.

(5) Empirical regressed relationships are proposed to describe the variations of the aerodynamic damping ratio associated with the acrosswind response of the downwind prism. Together with the histories of the base moment from the force-balance measurements, numerical calculations show that the predicted acrosswind tip responses of the downwind prism agree well with those from the measurements.

Acknowledgements

The study is cordially supported by the National Science Council (Grant No. NSC 98-2221-E-005-063-MY2).

References

Bailey, P.A. (1985), "Interference excitation of twin tall buildings", *J. Wind Eng. Ind. Aerod.*, **21,** 323-338.

Blazik-Borowa, E. (2006), "Interference loads of two cylinders in a side-by-side arrangement", *Wind Struct.*, **9**(1), 75-93.

Cheng, C.M., Lu, P.C. and Tsai, M.S. (2002), "Acrosswind aerodynamic damping of isolated square shaped buildings", *J. Wind Eng. Ind. Aerod.*, **90**(12-15), 1743-1756.
Gabbai, R.D. and Simiu E. (2010), "Aerodymic damping in the along-wind response of tall buildings", *J. Struct. Eng.- ASCE*, **136**(1), 117-119.
Huang, P. and Gu, M. (2005), "Experimental study on wind-induced dynamic interference effects between two tall buildings", *J. Wind Eng. Ind. Aerod.*, **8,** 147-161.
Khanduri, A.C., Stathopoulos, T. and Bédard, C. (1998), "Wind-induced interference effects on buildings - a review of the state-of-the art", *Eng. Struct.*, **20**(7), 617-630.
Kumar, R.A. and Gowda, B.H.L. (2006), "Flow-induced vibration of a square cylinder without and with interference", *J. Fluids Struct.*, **22**, 345-369.
Lim, J. and Bienkiewicz, B. (2007), "Wind-induced response of structurally coupled twin tall buildings", *Wind Struct.*, **10**(4), 383-398.
Matsumoto, T. (1986), "On the acrosswind oscillation of tall buildings", *J. Wind Eng. Ind. Aerod.*, **24**(1), 69-85.
Sakamoto, H. and Haniu, H. (1988), "Aerodynamic forces acting on two square prisms placed vertically in a turbulent boundary layer", *Wind Eng. Ind. Aerod.*, **31,** 41-85.
Taniike, Y. and Inaoka, H. (1988), "Aeroelastic behavior of tall buildings in wakes", *J. Wind Eng. Ind. Aerod.*, **28,** 317-327.
Taniike, Y. (1992), "Interference mechanism for enhanced wind forces on neighboring tall buildings", *J. Wind Eng. Ind. Aerod.*, **41-44,** 1073-1083.
Watanabe, Y., Isyumov, N. and Davenport, A.G. (1997), "Empirical aerodynamic damping function for tall building", *J. Wind Eng. Ind. Aerod.*, **72,** 313-321.
Zhang A. and Gu, M. (2008), "Wind tunnel tests and numerical simulations of wind pressures on buildings in staggered arrangement", *J. Wind Eng. Ind. Aerod.*, **96**(10-11), 2067-2079.

CC